IOP Publishing | Astro Ltd Laser Physics Letters
Laser Phys. Lett. **21** (2024) 045206 (8pp) https://doi.org/10.1088/1612-202X/ad2920

Letter

Orbital angular momentum sensing of composite vortex light in a single-layer graphene system

S I S Al-Hawary[1], Farag M A Altalbawy[2,3,*], C Rodriguez-Benites[4], A Kumar[5], Wesam R Kadhum[6,7], N Zaurbekova[8], H A Abbas[9], S J Shoja[10], A Alawadi[11,12,13] and R Sivaraman[14]

[1] Department of Business Administration, Business School, Al al-Bayt University, PO BOX 130040, Mafraq 25113, Jordan
[2] Department of Chemistry, University College of Duba, University of Tabuk, Duba 71911, Saudi Arabia
[3] National Institute of Laser Enhanced Sciences (NILES), University of Cairo, Giza 12613, Egypt
[4] Universidad César Vallejo, Chimbote, Peru
[5] Department of Nuclear and Renewable Energy, Ural Federal University Named after the First President of Russia Boris Yeltsin, Ekaterinburg 620002, Russia
[6] Department of Pharmacy, Kut University College, Kut, 52001 Wasit, Iraq
[7] Advanced Research Center, Kut University College, Kut, 52001 Wasit, Iraq
[8] Kazakh National Women's Teacher Training University Almaty Kazakhstan, Almaty, Kazakhstan
[9] College of Technical Engineering/ National University of Science and Technology, Dhi Qar, Iraq
[10] College of Health & Medical Technology, Al-Ayen University, Thi-Qar, Iraq
[11] College of Technical Engineering, The Islamic University, Najaf, Iraq
[12] College of Technical Engineering, The Islamic University of Al Diwaniyah, Al Diwaniyah, Iraq
[13] College of Technical Engineering, The Islamic University of Babylon, Babylon, Iraq
[14] Department of Mathematics Dwaraka Doss Goverdhan Doss Vaishnav College, Arumbakkam, Chennai, India

E-mail: f_altalbawy@yahoo.com

Received 22 January 2024
Accepted for publication 9 February 2024
Published 26 February 2024

Abstract

This paper explores the impact of orbital angular momentum (OAM) in composite vortex light on the absorption and dispersion characteristics of a weak probe light interacting with a single-layer graphene system. Through systematic investigation, we demonstrate the exceptional control achievable over absorption and dispersion profiles by manipulating the OAM of light. Under resonance conditions for the probe light, transparent regions emerge in the spatial profile of probe absorption, and the number of these transparent regions can be precisely regulated by adjusting the OAM number of the composite vortex light. Conversely, in the case of off-resonance probe light, amplified regions surface in the absorption spectrum, with the number of these regions controllable by the OAM state of the composite vortex light. These findings hold significant implications for optical communication systems, offering a valuable

* Author to whom any correspondence should be addressed.

tool for the detection and measurement of the OAM number of composite vortex light, and paving the way for advancements in tailored signal processing and communication technologies.

Keywords: orbital angular momentum, single layer graphene, composite vortex light

1. Introduction

The interaction between matter and light constitutes a foundational aspect of numerous optical phenomena in theoretical quantum optics. These encompass advancements such as large Kerr nonlinearity [1, 2], the optical solitons [3], the phenomenon of electromagnetically induced transparency (EIT) [4], the modified optical bistability [5], the dynamics inherent in four-wave mixing (FWM) [6, 7], and various others [8–12]. A pivotal requirement is the interaction between a light source and a material, which can span across diverse mediums [13–19]. When an atom engages with a field, the resulting atomic coherence emerges as a crucial mechanism, facilitating effective control and modulation of the optical properties within quantum systems [20–25].

The EIT in atomic systems has proven to be particularly advantageous for graphene-based systems, offering numerous theoretical and experimental applications [21, 26–28]. Graphene, characterized by a two-dimensional hexagon-shaped crystal structure composed of carbon atoms arranged in a single sheet, possesses unique optical and electrical properties. In proximity to the Dirac point or cones, these optical and electrical characteristics exhibit a linear dispersion [29, 30]. The graphene sheet, owing to its gapless band structure, demonstrates nonlinear behavior in the terahertz (THz) and infrared region (IR) [27, 31].

The orbital angular momentum (OAM) of light [32], on the other hand, imparts an additional layer of flexibility to optical technologies, unlocking a myriad of applications in various quantum technologies [33, 34]. OAM light takes the form of a vortex beam, characterized by a helical phase front and a ring-shaped intensity profile. Despite their roots predating 1992, Allen *et al* [35] pioneered the observation of such twisted light beams with helical wavefronts and a phase singularity, resulting in a dark spot with no intensity in the middle. Intriguing quantum optical phenomena, including second harmonic generation [36], FWM [37], sum-frequency generation [38], and spatially structured EIT [39], emerge when such structured light interacts with matter. Recent studies have utilized Laguerre–Gaussian beams to explore symmetric and asymmetric diffraction patterns in ensembles of three- and four-level atomic systems [40, 41]. It has been revealed that the Fraunhofer diffraction pattern in multi-level atomic systems is contingent on both the applied fields' OAM and their intensity profile [42].

This article introduces a graphene-based system designed for measuring the OAM state of a composite optical vortex field. Our investigation reveals that, owing to the radiation of THz signals, the probe absorption can be controlled across various regions, exhibiting a strong dependence on the OAM number of the vortex light. This dependence arises from distinct electrical characteristics and selection rules governing transitions between Landau levels near a Dirac point [26, 43, 44]. Consequently, a probe laser beam can generate a discernible nonlinear frequency even within a single monolayer of graphene. This allows for the identification of OAM in graphene's Landau level, presenting valuable implications for memory storage. We anticipate that our proposed graphene-based technology offers greater practical feasibility and utility in optical memory and sensor applications compared to previously published techniques.

2. Model and formulations

The diagrams presented in figures 1(a) and (b) illustrates the arrangement of Landau levels in a single-layer graphene (SLG) system interacting with laser fields. This specific configuration has previously been employed to investigate notable optical nonlinearity, nonlinear frequency conversion, generation of entangled photons, and the formation of ultraslow solitons, as referenced in [15, 26, 43–45]. By introducing an external magnetic field within the range of 0.01–10T, optical transitions between neighboring Landau levels (LLs) in graphene are expected to occur in the infrared to THz region. In the scenario of a monolayer graphene subjected to a magnetic field without the presence of an external optical field, the effective-mass Hamiltonian can be expressed as [29]:

$$\hat{H}_0 = v_F \begin{pmatrix} 0 & \hat{\pi}_x - i\hat{\pi}_y & 0 & 0 \\ \hat{\pi}_x + i\hat{\pi}_y & 0 & 0 & 0 \\ 0 & 0 & 0 & \hat{\pi}_x + i\hat{\pi}_y \\ 0 & 0 & \hat{\pi}_x - i\hat{\pi}_y & 0 \end{pmatrix}, \tag{1}$$

where $v_F = 3\gamma_0/(2\hbar a) \approx 10^6\, m/s$ (where $\gamma_0 \sim 2.8\, eV$ and $a = 1.42\, \overset{\circ}{A}$ represent the nearest-neighbor hopping energy and C–C spacing) is a band parameter denoting the Fermi velocity, $\hat{\vec{\pi}} = \hat{\vec{p}} + e\vec{A}/c$ denotes the generalized momentum operator, $\hat{\vec{p}}$ is the electron momentum operator, e is the electron charge, and $\vec{A}$ is the vector potential, equal to $(0, Bx)$ for a static magnetic field. We introduce the vector potential of the optical field ($\vec{A}_{\text{opt}} = ic\vec{E}/\omega$ and $\vec{E} = \vec{E}_p + \vec{E}_0$) to the vector potential of the magnetic field in the generalized momentum operator $\hat{\vec{\pi}}$ in the Hamiltonian when the SLG interacts with two electric control fields. Specifically, a coupling field with Rabi frequency Ω_k and a weak probe field with Rabi frequency Ω_p interact on transitions $|b\rangle \rightarrow |c\rangle$ and $|c\rangle \rightarrow |d\rangle$. Simultaneously, an intense driving laser field with Rabi frequency Ω_{TH} applied on

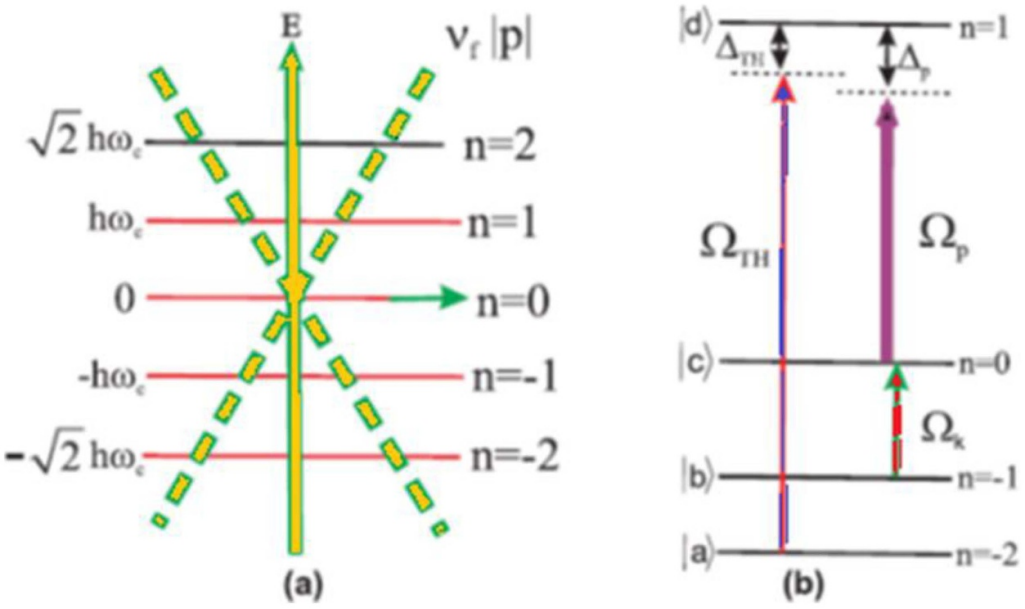

Figure 1. (a) Quantized energy levels (LLs) depicting electron and hole linear energy dispersion in the absence of a magnetic field near the Dirac point. (b) Landau levels of single layer graphene system interact by laser fields.

transition $|d\rangle \rightarrow |a\rangle$. The resulting interaction Hamiltonian can be expressed in the following form:

$$\hat{H}_{\text{int}} = v_F \vec{\sigma}.\frac{e}{c}\vec{A}_{\text{opt}}\,. \tag{2}$$

The density matrix for Dirac electrons in graphene, coupled to infrared laser fields, can be obtained by employing Liouville's equation $\frac{\partial\hat{\rho}}{\partial t} = -\frac{i}{\hbar}[\hat{H}_{\text{int}},\hat{\rho}] + \hat{R}(\hat{\rho})$. In this context $\hat{R}(\hat{\rho})$ represents incoherent relaxation, stemming from factors such as disorder, phonon interactions, and carrier-carrier interactions. As a result, the equations of motion for the density matrix in the four-level graphene system can be written as:

$$\begin{aligned}
\dot{\rho}_{dc} &= [i\Delta_p - \gamma_1]\,\rho_{dc} + \frac{i}{2}\Omega_{\text{TH}}\rho_{ac} + \frac{i}{2}\Omega_p\,(\rho_{cc} - \rho_{dd}) - \frac{i}{2}\Omega_k\rho_{db},\\
\dot{\rho}_{ac} &= [-i\,(\Delta_{\text{TH}} - \Delta_p) - \Gamma_p]\,\rho_{ac} + \frac{i}{2}\Omega_{\text{TH}}\rho_{dc} - \frac{i}{2}\Omega_p\rho_{ad} - \frac{i}{2}\Omega_k\rho_{ab},\\
\dot{\rho}_{ab} &= [-i\,(\Delta_{\text{TH}} - \Delta_p) - \gamma_3]\,\rho_{ab} + \frac{i}{2}\Omega_{\text{TH}}\rho_{db} - \frac{i}{2}\Omega_k\rho_{ac},\\
\dot{\rho}_{db} &= [i\Delta_p - \gamma_2]\,\rho_{db} + \frac{i}{2}\Omega_{\text{TH}}\rho_{ab} + \frac{i}{2}\Omega_p\rho_{cb} - \frac{i}{2}\Omega_k\rho_{dc}
\end{aligned} \tag{3}$$

where $\Delta_{\text{TH}} = (\varepsilon_{n=1} - \varepsilon_{n=-2})/\hbar - \omega_{\text{TH}}$ and $\Delta_p = (\varepsilon_{n=1} - \varepsilon_{n=0})/\hbar - \omega_p$ stand for the single-photon detunings, and $\varepsilon_n = \text{sgn}(n)\hbar\omega_c\sqrt{|n|}$ shoes the energy of the Landau level for electrons near the Dirac point, with $n = 0, \pm1, \pm2, \ldots, \omega_c = \sqrt{2}v_F/l_c$, and $l_c = \sqrt{\hbar c/eB}$ indicates the magnetic length. Also γ_1 is stimulated decay from $|d\rangle$ to $|c\rangle$, γ_2 shows decay from $|d\rangle$ to $|b\rangle$ and γ_3 represents decay from $|c\rangle$ to $|a\rangle$, where Γ_f is basically forbidden decay from $|c\rangle$ to $|a\rangle$. The set of equations represented by equation (3) can be reformulated into the concise form of a single differential matrix equation [2]

$$\dot{K} = -MK + C \tag{4}$$

where K and C are column vectors and M is the matrix of coefficients. The formal solution of such an equation is given by

$$K(t) = \int_{-\infty}^{t} e^{-M\left(t-t'\right)}Cdt' = M^{-1}C. \tag{5}$$

We employ the aforementioned equation to derive the steady-state solution for ρ_{dc} as follows:

$$\rho_{dc} = \frac{i\,[i\Omega_{\text{TH}}\alpha_1 + \alpha_2\,(-i\Delta_p + \gamma_3)]}{A}, \tag{6}$$

where

$$A = i\Omega_{\text{TH}}\alpha_3 + (\gamma_3 + i\Delta_{\text{TH}} - i\Delta_p)\,\alpha_4\,(-i\Delta_p + \gamma_3) + i\Omega_k\alpha_5, \tag{7}$$

and

$$\begin{aligned}
\alpha_1 &= -i\Gamma_f\Omega_{\text{TH}} + \Delta_{\text{TH}}\Omega_{\text{TH}} - \Delta_p\Omega_{\text{TH}},\\
\alpha_2 &= (\Gamma_f + i\Delta_{\text{TH}} - i\Delta_p)\,(\gamma_3 + i\Delta_{\text{TH}} - i\Delta_p) + \Omega_k^2,\\
\alpha_3 &= -\Gamma_f\Delta_p\Omega_{\text{TH}} - i\Delta_{\text{TH}}\Delta_p\Omega_{\text{TH}} + i\Delta_p^2\Omega_{\text{TH}} - i\Omega_{\text{TH}}^3\\
&\quad + i\Omega_{\text{TH}}\Omega_k^2 - i\Gamma_f\Omega_{\text{TH}}\gamma_1 + \Delta_{\text{TH}}\Omega_{\text{TH}}\gamma_1 - \Delta_p\Omega_{\text{TH}}\gamma_1,\\
\alpha_4 &= i\Omega_k\,(-i\Gamma_f\Omega_k + \Delta_{\text{TH}}\Omega_k - \Delta_p\Omega_k)\\
&\quad + \left(\Omega_{\text{TH}}^2 + \Gamma_f + i\Delta_{\text{TH}} - i\Delta_p\right)(-i\Delta_p + \gamma_1)\,,\\
\alpha_5 &= i\Omega_{\text{TH}}^2\Omega_k - i\Omega_k\left(\Omega_k^2 + (-i\Delta_p + \gamma_1)\,(-i\Delta_p + \gamma_3)\right).
\end{aligned} \tag{8}$$

Indeed, it is established that the imaginary component of the coherence term signifies absorption, whereas the real part is indicative of dispersion. Specifically, a positive imaginary part denotes absorption, while a negative value implies gain. This fundamental relationship between the coherence term and absorption/gain provides valuable insights into the behavior of

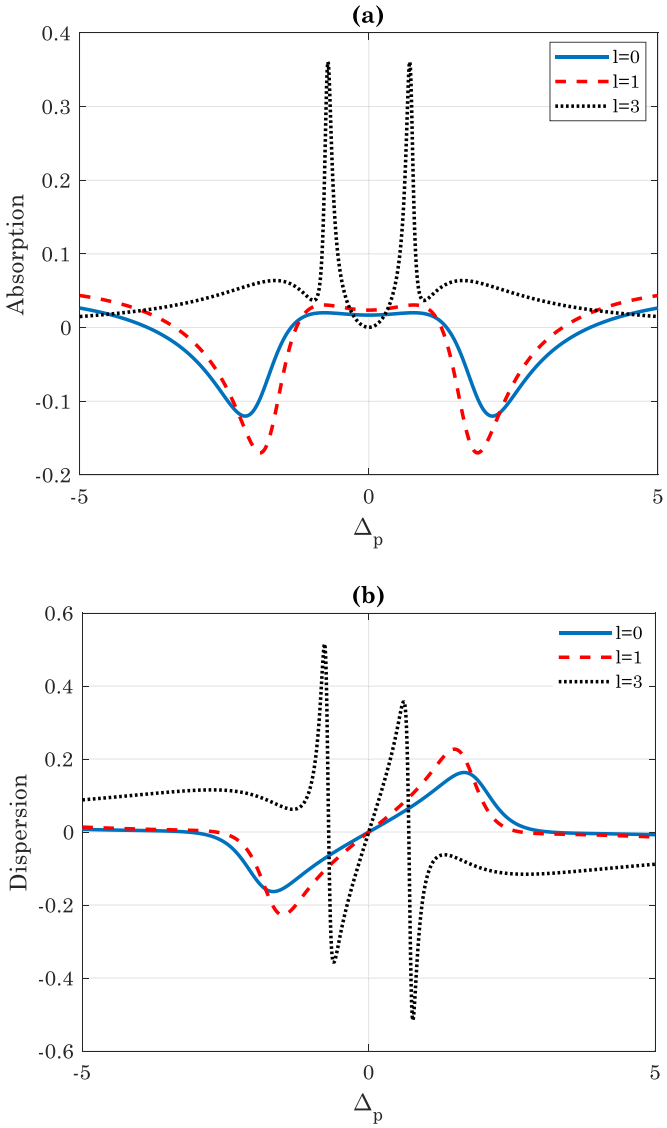

Figure 2. Absorption (a) and dispersion (b) properties of the medium versus probe detuning for solid line $l = 0$, dashed line $l = 1$ and dotted line $l = 3$. The selected parameters are $\Gamma_f = 0.002$, $\gamma_1 = 1$, $\gamma_2 = 0.1$, $\gamma_3 = 0.2$, $\Delta_{\mathrm{TH}} = 0$, $r/w = 1$, $\varepsilon_k = 5$, $\Omega_{\mathrm{TH}} = 1$ and $\phi = \pi/6$.

the system under consideration. Such understanding is pivotal for interpreting and manipulating the optical characteristics of the proposed system, offering avenues for tailored control in diverse applications, ranging from amplification to dispersion engineering.

3. Results and discussion

In the following, we replace the coupling field Ω_k by a composite vortex light of the form:

$$\Omega_k = \Omega e^{-r^2/\omega^2}\left[(r/\omega)^{|l_1|}e^{il_1\phi} + (r/\omega)^{|l_2|}e^{il_2\phi}\right] \tag{9}$$

where, we have $l_1 = -l_2 = l$. Then we have for equation (9):

$$\Omega_k = \varepsilon_k \cos(l\phi) \tag{10a}$$

$$\varepsilon_k = 2\Omega e^{-r^2/\omega^2}(r/\omega)^{|l|} \tag{10b}$$

where l corresponds to the OAM, ϕ denotes the azimuthal angle and r shows the radial distance of the vortex light. In figure 2, we present the absorption (a) and dispersion (b) characteristics of the medium against the detuning of the probe light. Notably, for $l = 0$ and at $\Delta_p \approx \pm 2.5$, the absorption curve exhibits a negative value, emphasizing an amplification of the probe field in these frequency regions. This behavior is particularly pronounced around the resonant frequency $\Delta_p = 0$, where the absorption value turns positive. Upon closer examination, it is evident that for $l = 1$ (dashed line), the absorption spectrum retains a similar profile, with the gain value experiencing an increase in frequency regions away from the resonance. However, for $l = 3$ (dotted line), the absorption spectrum undergoes a substantial change, manifesting a positive value throughout all frequency regions. This signifies that in these areas, the probe light is absorbed within the graphene system. The modulation of the l value serves as a mechanism for controlling the dispersion behavior of the system. By adjusting l the slope of the dispersion curve

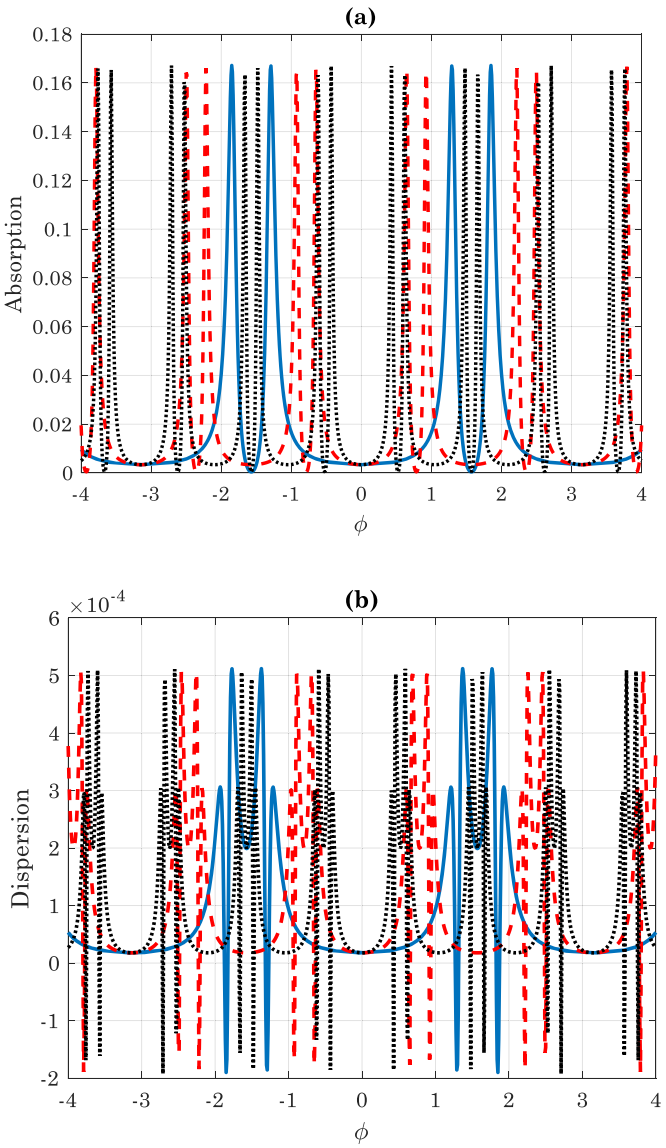

Figure 3. Absorption (a) and dispersion (b) properties of the medium versus azimuthal angle ϕ in resonance condition of the probe light ($\Delta_p = 0$). The solid line $l = 1$, dashed line $l = 2$ and dotted line $l = 3$. The selected parameters are same as figure 2.

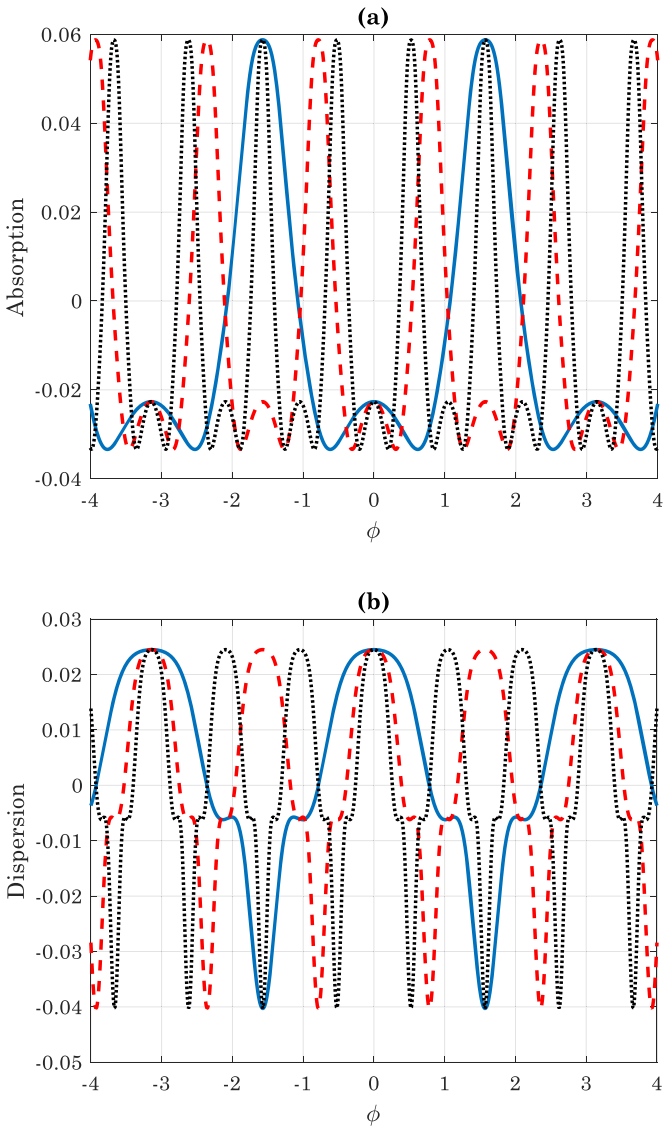

Figure 4. Absorption (a) and dispersion (b) properties of the medium versus azimuthal angle ϕ in off-resonance condition of the probe light ($\Delta_p = 2.5$). The solid line $l = 1$, dashed line $l = 2$ and dotted line $l = 3$. The selected parameters are same as figure 2.

undergoes noticeable changes, particularly in frequency regions distant from the resonance. This implies the capability to influence the group velocity by altering the l value in these specific frequency areas. This observation suggests a versatile control over absorption and dispersion behaviors, paving the way for tailored applications in manipulating and harnessing light-matter interactions within the graphene-based system. Further exploration and fine-tuning of these parameters could lead to advancements in optoelectronic devices and quantum technologies.

In figure 3, the absorption (a) and dispersion (b) spectra are presented in relation to the azimuthal phase of the vortex light. Assuming resonance between the probe field and the corresponding transition, it becomes evident that the absorption spectrum attains zero values at different phases by manipulating the OAM value. This observation underscores the potential to achieve a transparent medium for the probe field in the resonant frequency region through meticulous control of both the OAM and azimuthal phase parameters. Furthermore, the dispersion behavior exhibits tunability, showcasing the capacity to control it for various OAM values and azimuthal angles. This dual control over absorption and dispersion characteristics offers a promising avenue for tailoring the optical response of the system. Such tunability is crucial for advancing applications that demand precision in managing light-matter interactions, ranging from transparent media creation to the design of customizable photonic devices.

In figure 4, we depict the compelling behaviors of the absorption (a) and dispersion (b) spectra when the probe field

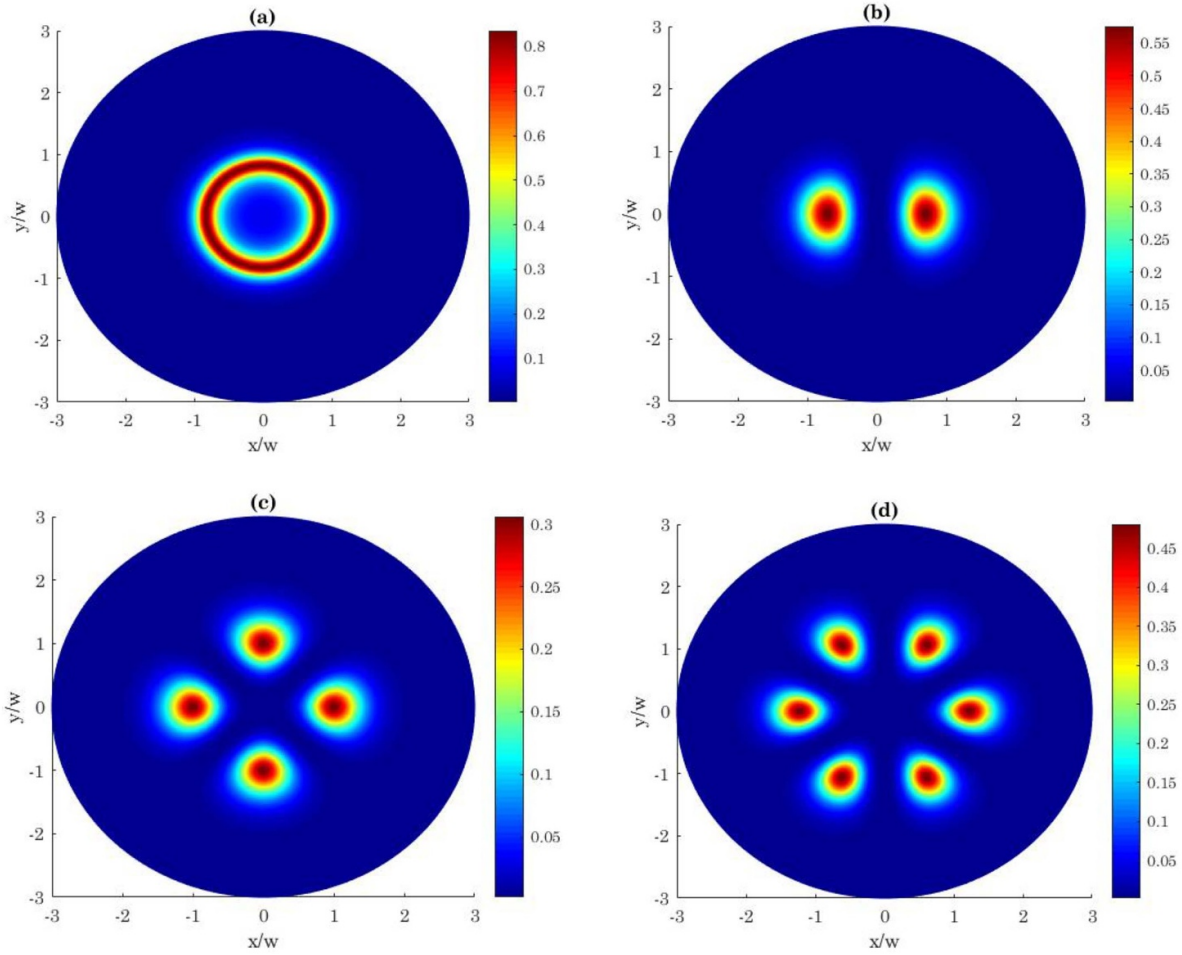

Figure 5. Spatial dependent of the probe absorption versus *x/w, y/w* in the resonance condition of the probe light ($\Delta_p = 0$). $l = 0$ (a), $l = 1$ (b), $l = 2$ (c) and $l = 3$ (d). The selected parameters are same as figure 2.

is considerably detuned from the resonance frequency ($\Delta_p = 2.5$), presented in terms of the azimuthal angle. Notably, in this scenario, the absorption spectrum of the probe field exhibits negative values across various azimuthal angles, signifying robust signal amplification within the environment. This intriguing finding underscores the potential for achieving significant signal enhancement even when the probe frequency is far from resonance. Moreover, the dispersion spectrum reveals a pronounced dependence on the light-dependent parameters of the vortex light in these conditions. This inherent dependency enables precise control over the group velocity of the probe light. This level of tunability in the group velocity, particularly in the context of amplified probe fields, holds great significance for applications demanding controlled signal amplification and manipulation of the propagation characteristics in advanced photonic systems.

In the subsequent analysis, explored in figures 5 and 6, we delve into the spatial intricacies of the absorption spectrum across various OAM values. Figure 5 scrutinizes the spatial dependence when the probe field resonates with its transition, while figure 6 investigates the scenario where the probe field is far from resonance.

In figure 5(a), with $l = 0$ (part (a) of figure 5), a distinct ring emerges in the absorption spectrum. Encircling this ring, the absorption values are notably higher than in the surrounding regions, indicating enhanced absorption. Transitioning to figure 5(b) with $l = 1$ (part (b) of figure 5), two distinct spots appear in the absorption spectrum, with heightened absorption at their center. As the OAM parameter increases to 2 and 3 (figures 5(c) and (d)), the number of spots escalates to 4 and 6, respectively, all characterized by the highest absorption values.

Contrastingly, in figure 6, where the probe field is in a non-resonant state with its transition, the spatial pattern of the absorption spectrum evolves with varying *l*. The crucial distinction lies in the negative absorption values at the center of these spots. In these regions, the probe field undergoes amplification, signifying the environment's role as an amplifier.

This spatial exploration not only enriches our understanding of absorption dynamics but also provides insights into tailoring light-matter interactions for applications such as spatially controlled amplification and signal enhancement in diverse photonic systems.

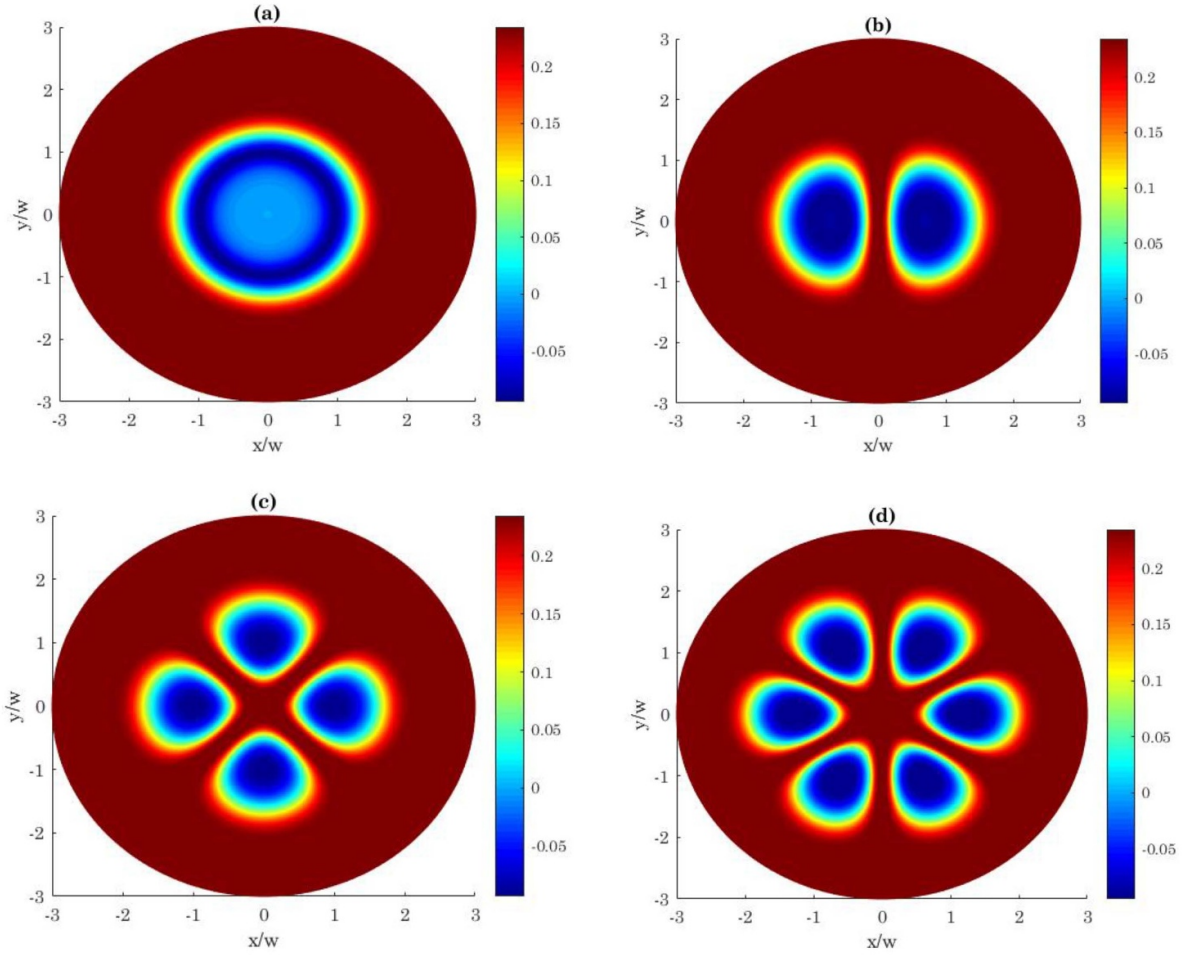

Figure 6. Spatial dependent of the probe absorption versus *x/w, y/w* in the off- resonance condition of the probe light ($\Delta_p = 2.5$). $l = 0$ (a), $l = 1$ (b), $l = 2$ (c) and $l = 3$ (d). The selected parameters are same as figure 2.

4. Conclusion

In conclusion, this study has delved into the influence of OAM in composite vortex light on the absorption and dispersion characteristics of a weak probe light interacting with a SLG system. The key findings highlight the remarkable control achievable over absorption and dispersion profiles through the manipulation of the OAM of light.

Under resonance conditions for the probe light, we observed the emergence of transparent regions in the spatial profile of probe absorption. The number of these transparent regions proved adjustable by varying the OAM number of the composite vortex light. Conversely, in the case of off-resonance probe light, amplified regions surfaced in the absorption spectrum. Remarkably, the number of amplified regions could also be controlled by the OAM state of the composite vortex light.

These results unveil promising avenues for applications in optical communication systems, where the detection and measurement of the OAM number of composite vortex light are crucial. By leveraging the controllable absorption and dispersion behaviors demonstrated in this study, advancements in tailored signal processing and communication technologies may be achieved.

References

[1] Sahrai M, Asadpour S H and Sadighi R 2010 *J. Nonlinear Opt. Phys. Mater.* **19** 503–15
[2] Asadpour S H and Soleimani H R 2012 *Coherent Opt. Phenom.* **1** 1–6
[3] Wu Y and Deng L 2004 *Phys. Rev. Lett.* **93** 143904
[4] Wu Y and Yang X 2005 *Phys. Rev.* A **71** 053806
[5] Shiri J, Khalilzadeh J and Asadpour S H 2021 *Laser Phys.* **31** 036202
[6] Wu Y, Saldana J and Zhu Y 2003 *Phys. Rev.* A **67** 013811
[7] Wu Y and Yang X 2004 *Phys. Rev.* A **70** 053818
[8] Asadpour S H, Faizabadi E, Kudriašov V, Paspalakis E and Hamedi H 2021 *Eur. Phys. J. Plus* **136** 1–13
[9] Vafafard A, Sahrai M, Siahpoush V, Hamedi H R and Asadpour S H 2020 *Sci. Rep.* **10** 1–13
[10] Li H, Tang J, Kang Y, Zhao H, Fang D, Fang X, Chen R and Wei Z 2018 *Appl. Phys. Lett.* **113** 233104
[11] Fan X, Wei G, Lin X, Wang X, Si Z, Zhang X, Shao Q, Mangin S, Fullerton E and Jiang L 2020 *Matter* **2** 1582–93
[12] Wei G, Lin X, Si Z, Wang D, Wang X, Fan X, Deng K, Liu K, Jiang K and Lei N 2020 *Adv. Quantum Technol.* **3** 1900104

[13] Wu Y and Yang X 2007 *Phys. Rev.* B **76** 054425
[14] Yang W-X, Chen A-X, Lee R-K and Wu Y 2011 *Phys. Rev.* A **84** 013835
[15] Ding C, Yu R, Li J, Hao X and Wu Y 2014 *Phys. Rev.* A **90** 043819
[16] Si L-G, Xiong H, Zubairy M S and Wu Y 2017 *Phys. Rev.* A **95** 033803
[17] Zhao J, Gao J, Li W, Qian Y, Shen X, Wang X, Shen X, Hu Z, Dong C and Huang Q 2021 *Nat. Commun.* **12** 1–9
[18] Chen Y, Long J, Xie B, Kuang Y, Chen X, Hou M, Gao J, Liu H, He Y and Wong C-P 2022 *ACS Appl. Mater. Interfaces* **14** 4647–55
[19] Fu Q, Si L, Liu J, Shi H and Li Y 2022 *Appl. Opt.* **61** 6330–8
[20] Chen F 2023 *Laser Phys. Lett.* **20** 095206
[21] Saeed S H, Lafta H A, Abbass R, Fahim F S, Adhab A H, Shams M A, Kadhim A A and Gatea M A 2023 *Laser Phys.* **33** 045202
[22] Zhang X, Li L, Wang X and Zheng L 2022 *Laser Phys. Lett.* **19** 035203
[23] Li J, Li J, Yu R and Wu Y 2015 *Laser Phys. Lett.* **12** 085201
[24] Jafarzadeh H, Asadpour S H and Soleimani H R 2015 *Laser Phys.* **25** 035201
[25] Wang Z, Zhen S and Yu B 2015 *Laser Phys. Lett.* **12** 046004
[26] Yu R, Zhang D, Ding C, Huang H, Sun Z and Yang X 2016 *Laser Phys. Lett.* **13** 125201
[27] Liu S, Liu S, Zhu Z and Yang W-X 2016 *Laser Phys.* **26** 035401
[28] Asadpour S H and Soleimani H R 2015 *Laser Phys. Lett.* **13** 015201
[29] Tokman M, Yao X and Belyanin A 2013 *Phys. Rev. Lett.* **110** 077404
[30] Yao X and Belyanin A 2013 *J. Phys. Condens. Matter* **25** 054203
[31] Shi C, He X, Peng J, Xiao G, Liu F, Lin F and Zhang H 2019 *Opt. Laser Technol.* **114** 28–34
[32] Lembessis V E, Ellinas D, Babiker M and Al-Dossary O 2014 *Phys. Rev.* A **89** 053616
[33] Zhang Z, Ma D, Zhang Y, Cao M, Xu Z and Zhang Y 2017 *Opt. Lett.* **42** 1059–62
[34] Hamideh Kazemi S and Mahmoudi M 2019 *Laser Phys. Lett.* **16** 076001
[35] Allen L, Beijersbergen M W, Spreeuw R and Woerdman J 1992 *Phys. Rev.* A **45** 8185
[36] Biss D and Brown T 2003 *Opt. Lett.* **28** 923–5
[37] Hong Y, Wang Z, Ding D and Yu B 2019 *Opt. Express* **27** 29863–74
[38] Zhang D, Liu X, Yang L, Li X, Zhang Z and Zhang Y 2017 *Opt. Lett.* **42** 3097–100
[39] Hamedi H R, Kudriasov V, Ruseckas J and Juzeliunas G 2018 *Opt. Express* **26** 28249–62
[40] Liu Y, Xiang Y and Mohammed A A 2022 *Laser Phys. Lett.* **19** 095205
[41] Asadpour S H, Hamedi H R, Kirova T and Paspalakis E 2022 *Phys. Rev.* A **105** 043709
[42] Asadpour S H, Kirova T, Qian J, Hamedi H R, Juzeliūnas G and Paspalakis E 2021 *Sci. Rep.* **11** 1–11
[43] Chen H-J, Sun B-B, Wu H-W and Fang X-W 2017 *Eur. Phys. J.* D **71** 67
[44] Ding C, Yu R, Hao X, Zhang D and Zu F 2017 *J. Appl. Phys.* **121** 214301
[45] Ding C, Yu R, Yang X, Zhang D and Huang M 2015 *Eur. Phys. J.* D **69** 263